

Milky Way Dynamics using GAIA DR3 Data

P. Rosselló^{1,*}

We provide a simplified proof-of-concept examination of orbital dynamics of different components of the Milky Way using GAIA DR3 data to gain insight into the galaxy's kinematic structure. This work is presented as an assignment for the subject *Física Galáctica* within the Astrophysics Master's program at Universidad de La Laguna. We retrieved GAIA DR3 data to create sample of $\sim 1.8 \times 10^4$ stars reflective of the Milky Way's mass density distribution across its bulge, disk, and halo components. We adopted a simplified potential model of the Milky Way to integrate star orbits up to 500 Myr, with GAIA positions and velocities data serving as initial conditions. Our analysis results in distinctive behavioral patterns. Bulge stars show concentrated non-closed orbits with high eccentricities and angular momentum variations. Disk-component orbits are more stable and present minimal vertical excursions with respect to the galactic plane. Halo stars presented high spread in eccentricity, with substantial apocentric distances, suggesting a dynamically heated and dispersed component.

1 Introduction

The GAIA mission, launched by the European Space Agency in 2013 [Prusti et al., 2016], represents a milestone in astrometry. Gaia's third data release (DR3) [Creevey et al., 2023] has expanded astronomical research, helping among other things in identifying new solar system objects [Brown et al., 2021], delineating dark matter distribution [Buch et al., 2019]; and since the inclusion of radial velocity measurement in Gaia DR2 [Brown et al., 2021], the 6-dimensional information about the position and velocity of GAIA have been a key resource for enhancing our knowledge about the dynamics of our Galaxy [Nitschai et al., 2020, 2021].

This rich dataset enables precise initial condition settings for dynamic simulations of the Milky Way. However, to effectively simulate galactic dynamics, a robust model of gravitational interactions is necessary. Contemporary high-resolution hydrodynamical simulations, which integrate dark matter and baryonic particles, represent the state of the art in simulating galaxies, albeit with significant computational demands (see for example [Maccio et al., 2011]). In this study, we adopt a simpler yet effective approach, using instead a static potential to model the Milky Way's gravitational potential and integrate the orbits of a selected sample of GAIA stars. This approach, while idealized, allows for precise characterization of stars from the bulge, disk and halo of the Milky Way by discerning their kinematic properties. This work serves also as a proof-of-concept for the retrieval of GAIA data in galactocentric coordinates in a way that the resulting distribution of stars is representative of the star dis-

tribution within the Galaxy, effectively building a "toy Milky Way model".

2 Methodology

2.1 Smoothed Potential Approximation

In the context of N-body gravity simulations, achieving computational precision and efficiency often requires simplifications. In utmost rigor, in an N-body gravity simulation one would have to solve Newton's second law for each pair of mutually interacting bodies at each time step. This results in $N(N - 1)/2$ operations per time step, where N is the number of interacting bodies. The computational complexity grows as $\mathcal{O}(N^2)$ and becomes intractable for large N . To put this in perspective, for the desktop computer used for the subsequent analysis, with a 6-core AMD Ryzen 5 5600H processor running at 3.4GHz, simulating 100,000 bodies for 1000 time steps using a Verlet Step and Python's numba performance enhancer would take approximately 100 days, a prohibitive amount of time to anyone having to meet a deadline. While supercomputing resources can optimize this process significantly, even current capabilities fall short (by an order of magnitude) of simulating the Milky Way's estimated 100 billion stars within a reasonable time-frame.

A workaround to this problem is possible by means of a smoothed-potential approach. We assign a constant and continuous mass distribution to our Galaxy, and integrate the orbits of single stars with respect to the

¹Universidad de La Laguna

*alu0101693057@ull.edu.es

Galaxy's resulting potential. This approach is valid as long as the mass distribution is smooth and the stars are not massive enough to affect the gravitational field, which are both good approximations for the Milky Way [Bovy, 2023].

We use the `gala` Python package [Price-Whelan, 2017] to define the Milky Way's potential¹. We adopt a four-component model consisting of a Hernquist bulge and nucleus [Hernquist, 1990], a Miyamoto-Nagai disk [Miyamoto and Nagai, 1975], and an NFW halo [Navarro et al., 1997]. The total potential is

$$\Phi(\mathbf{r}) = \Phi_{\text{halo}}(\mathbf{r}) + \Phi_{\text{disk}}(\mathbf{r}) + \Phi_{\text{bulge}}(\mathbf{r}) + \Phi_{\text{nucleus}}(\mathbf{r}). \quad (1)$$

Expressions for each component are given in galactocentric coordinates in the Appendix. The resulting density distribution coming from this potential can be obtained by solving Poisson's equation

$$\nabla^2 \Phi(\mathbf{r}) = 4\pi G \rho(\mathbf{r}), \quad (2)$$

and is shown in Figure 1.

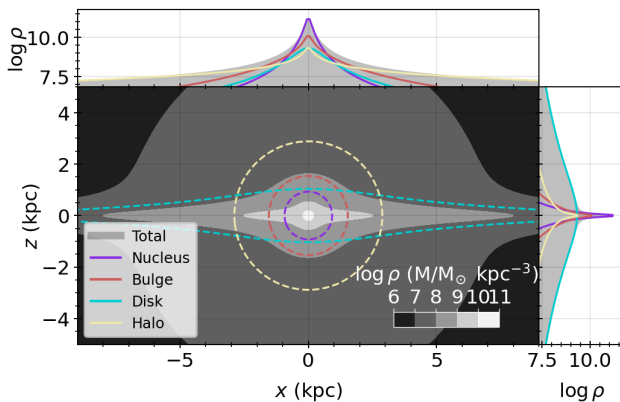


Figure 1: Mass density distribution of the Milky Way model in units $M/M_{\odot} \text{ kpc}^{-3}$. The main plot presents the density in the xz plane, with superimposed isopionical contours (dashed lines) at a density of $7.5 M_{\odot} \text{ kpc}^{-3}$ for each component: nucleus (purple), bulge (red), disk (blue), and halo (yellow). The top and right subplots display the marginal density profiles along the x and z axes, respectively, with colors corresponding to each galactic component.

The use of this potential model will be two-fold. On one hand, the potential will be used to integrate the orbits of stars using GAIA DR3 three-dimensional positions and velocities as initial conditions. On the other hand, we will use the resulting mass density $\rho(\mathbf{r})$ to weight our GAIA DR3 data sample, such that the resulting stellar distribution matches the mass density distribution of the Milky Way model. For this last step,

we will be assuming that the mass density distribution is a good proxy for the stellar density distribution.

2.2 GAIA Data Retrieval

We retrieved a sample of stars from GAIA's DR3 [Valenari et al., 2023, Prusti et al., 2016] representative of the Milky Way's mass density distribution across its bulge, disk, and halo components. The Gaia archive was accessed through ADQL queries via python script using the astropy library [Robitaille et al., 2013]. We are interested only in stars with full 6D phase-space information, so our sample would be limited to stars with measured radial velocity components.

GAIA queries must be made either in equatorial (RA, dec) or galactic (l, b) coordinates. On the other hand, we want to use our model's mass density $\rho(\mathbf{r})$ in galactocentric coordinates to weight our queries. We found that querying a representative sample of stars for our Galaxy's stellar distribution was a non-trivial task, due to the necessary coordinate transformations and fact that GAIA stars are concentrated around the solar neighborhood. To overcome this issue, we followed the following steps to retrieve representative samples of stars for the bulge, disk and halo components:

1. We defined Cartesian volume elements for each galactic component. The volume elements were defined as follows:
 - Bulge: A $0.5 \times 0.5 \times 0.5 \text{ kpc}^3$ cube centered at the origin.
 - Disk: 49 rectangular boxes with dimensions $2 \times 2 \times 0.6 \text{ kpc}^3$ defining a 0.6 kpc thickness disk at $z = 0$ with an approximate radius of 11.4 kpc.
 - Halo: 90 cubes with $3 \times 3 \times 3 \text{ kpc}^3$ dimensions defining a spherical halo with a radius of 11.4 kpc, with the exception of regions within 1 kpc of the disk, which were excluded.

Regions where limited to $x < 0$, as this is the side of the Milky Way where the Sun is located and more high quality GAIA data is available. This cartesian volumes are depicted in Figure 5 (left panel).

2. We transformed the vertices of each cartesian volume element in galactocentric coordinates (x, y, z) to galactic coordinates to get the corresponding (ϖ, l, b) vertices, where ϖ is the parallax. We then define the best match for the spher-

¹<https://gala-astro.readthedocs.io/en/v1.3/potential/define-milky-way-model.html>

ical volume elements in galactic coordinates plus parallax to be queried via ADQL.

3. We select a maximum number of $N = 10^5$ stars and we then weighted the number of stars of the query of each box by the mass density $\rho(\mathbf{r})$ of the Milky Way model integrated inside the box. This ensures that the number of stars retrieved for each component is proportional to the mass density of the Milky Way model.

After these steps, we refined the dataset by implementing a series of filters to ensure the astrometric and photometric integrity of the data. The filters applied, in GAIA's database nomenclature, are:

- `parallax_over_error > 2`: To select for data with a high signal-to-noise ratio in parallax measurements, enhancing the reliability of distance estimations.
- `astrometric_excess_noise < 1`: Excludes sources with significant unmodeled noise.
- `phot_rp_mean_flux_over_error > 2` and `phot_bp_mean_flux_over_error > 2`: Ensures more accurate photometric data.

Using this approach we found the number of stars in the bulge to be our limiting factor. After filtering, only 1660 stars (with radial velocities) were retrieved in the bulge. We then adjusted the number of stars in the disk and halo accordingly such that the final sample is representative of the mass density of our Galaxy. The resulting number of stars for each component were $N_{\text{bulge}} = 1660$, $N_{\text{disk}} = 8327$ and $N_{\text{halo}} = 7734$. The resulting stellar distribution for each component is shown in Figure 5 (center panel). The corresponding marginal profiles in galactocentric cylindrical coordinates are shown in Figure 5 (right panel). By looking at Figure 5 top-right panel we find that close to no stars where found at $|z| \lesssim 0.25$ kpc in the bulge. An expected result given the high extinction close to the galactic plane.

Finally, although we have relied on a simplistic distance estimation to retrieve our sample of stars, setting the solar-system barycentric radial distance to be $d = 1/\varpi$, where ϖ is the measured parallax, we can do a post-sampling refinement of our distance estimates using a Bayesian approach as detailed in Luri et al. [2018]. This method is particularly crucial for stars in the bulge and halo of the Milky Way, which are relatively far from us and thus often have large parallax errors. Although our initial

selection confined the parallax error to be at most half the measured value, these distant stars still require a more sophisticated statistical method for accurate distance derivation from parallax measurements. Details on the methodology and prior distributions used can be found in the source code repository. Specifically in https://github.com/pererossello/MW_toy_model/blob/main/code/utils.py.

2.3 CM Diagrams

Figure 3 presents color-magnitude (CM) diagrams for the bulge, disk, and halo. The diagrams show stellar populations before and after corrections for extinction and reddening, with gray points indicating uncorrected stellar data. However, not all stars have extinction and reddening corrections available. Notably, the disk and bulge populations exhibit pronounced reddening and extinction effects. The first realization comes from the concentration of very luminous stars with $M_G \gtrsim 0$ for all galactic components, potentially giants and supergiants. While a vague main sequence is discernible within the disk's diagram, it is non-existent for the bulge and halo populations. This observed distribution may result from a combination of observational biases inherent to GAIA data and the filtering criteria applied, which favors large intrinsic luminosities when selecting very distant stars with small apparent magnitudes and low photometric and astrometric errors.

3 Results

We set an integration time $T = 500$ Myr and a time step $\Delta t = 0.5$ Myr for the integration of our collected sample of stars. Integration was performed by applying the Milky Way potential defined in Eq. (1) and using the smoothed potential approximation and gala package's efficient capabilities.

Snapshots of the star's positions at $t = 0, 250$ and 500 Myr are represented in Figure 4. As expected from the initial conditions and the potential used, the initial binned distribution as retrieved from GAIA is smoothed out in a single spiral pattern at increasing integration time. A rendered video version of the simulation is available at https://github.com/pererossello/MW_toy_model/blob/main/toy_MW_model.mp4.

The orbital density projections and marginal profiles for the Milky Way's bulge, disk, and halo components

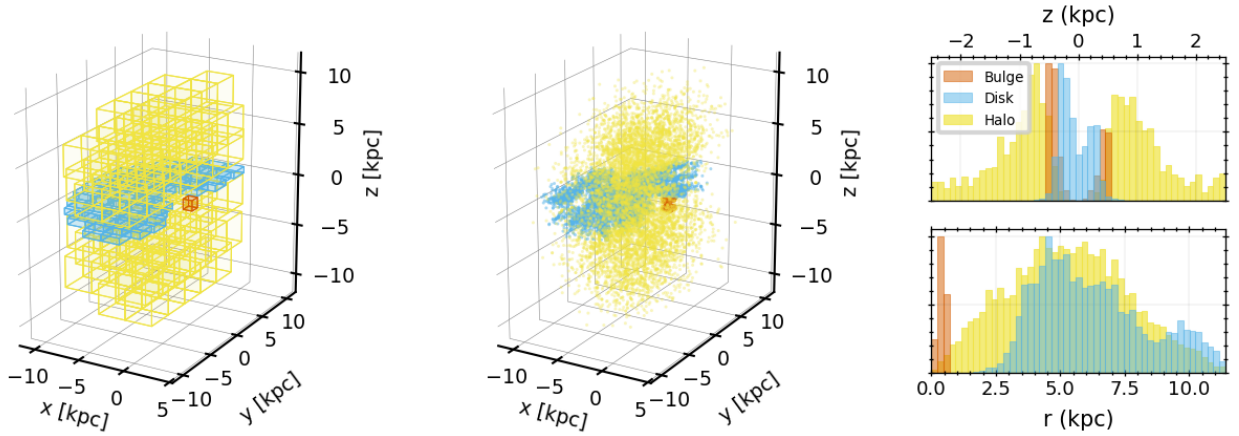


Figure 2: Galactic component distributions derived from GAIA DR3 data. Colors red, blue, and yellow correspond respectively to the bulge, disk, and halo of the Milky Way. Left: Cartesian volume elements defining the spatial selection criteria for querying the data of each component. Center: Post querying results after filtering and adjusting the number of stars of each galactic component to match the density distribution of the Milky Way. Right: Density profiles in cylindrical coordinates of the galactic components for the queried data in vertical (top) and cylindrical radial (bottom) dimensions.

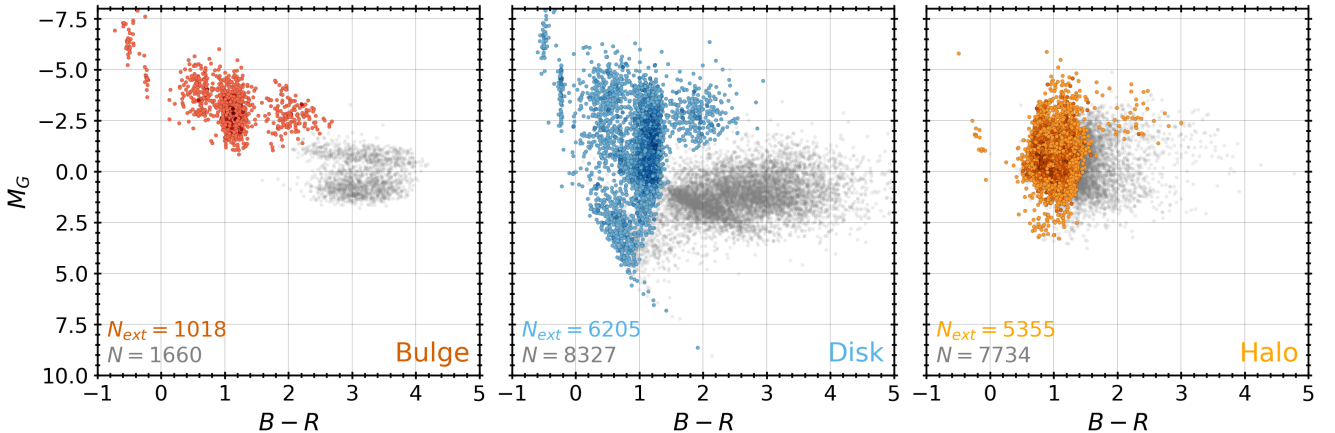


Figure 3: CM diagrams for the Milky Way's bulge (left, red), disk (center, blue), and halo (right, orange). The gray points in each plot represent stellar data prior to correction for extinction and reddening. The colored points have been corrected for these effects. The number of stars with extinction and reddening corrections (N_{ext}) is indicated for each component, alongside the total number of stars (N) in that component's sample.

after an integration period of 500 Myr are shown in Figure 5. To obtain an orbital density projection we define a binned plane (XY or XZ) and sum-up the number of stars in each bin for all integration time-steps. The result is a 2D histogram displaying a heatmap of the star density during the whole integration period, with units being star-count \times yr \times kpc $^{-2}$. The bulge exhibits a tightly concentrated distribution, indicating a relatively stable, dense center with orbits that show minimal dispersion. The disk orbits show a pronounced flat circular pattern, with a ten-fold difference between X-Z spatial dispersion and Z spatial dispersion. The halo is characterized by a broader and roughly spherical distribution, in accordance with the halo's diffuse and dynamically heated nature.

We computed estimates for the eccentricity, pericenter, apocenter, and maximum vertical height (z_{max}) reached above the galactic plane for each star in each galactic component. Although these values are not strictly well defined for a non-closed and non-periodic orbit, an approximate value provides a useful characterization of the orbital structure of each component. Pericenters and apocenters are computed by finding radial local minima and maxima of an orbit and taking its average. The vertical height z_{max} is computed in an analogous way. Results are displayed in Figure 6 for the bulge, disk, and halo populations. The bulge exhibits high eccentricity orbits with constrained pericenter and apocenter distances, along with minimal vertical extents. The disk presents more circular

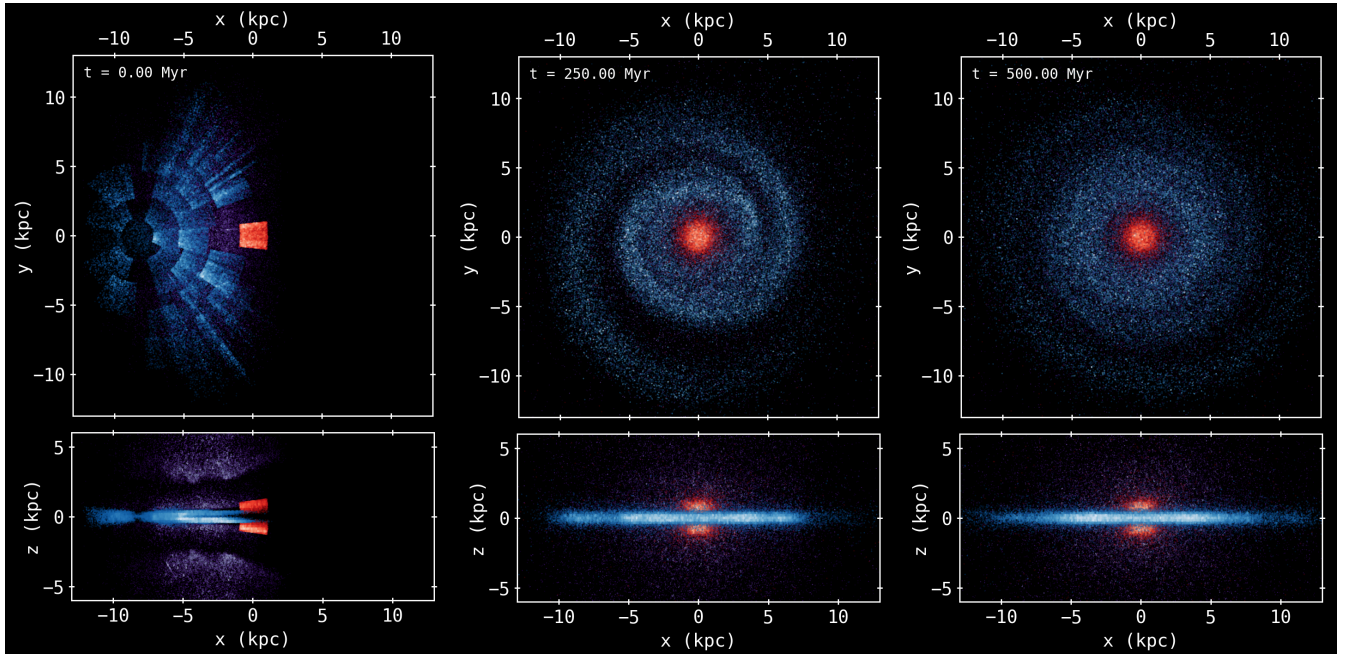


Figure 4: Snapshots of the simulated 17721 star orbits for $t = 0, 250, 500$ Myr indicating the dynamical evolution over time. The top row depicts the face-on view, and the bottom row shows the edge-on view of the galaxy. Red, blue, and purple correspond to the bulge, disk and halo components respectively. The snapshot at $t = 0$ Myr represents the initial conditions of the orbits as retrieved from GAIA.

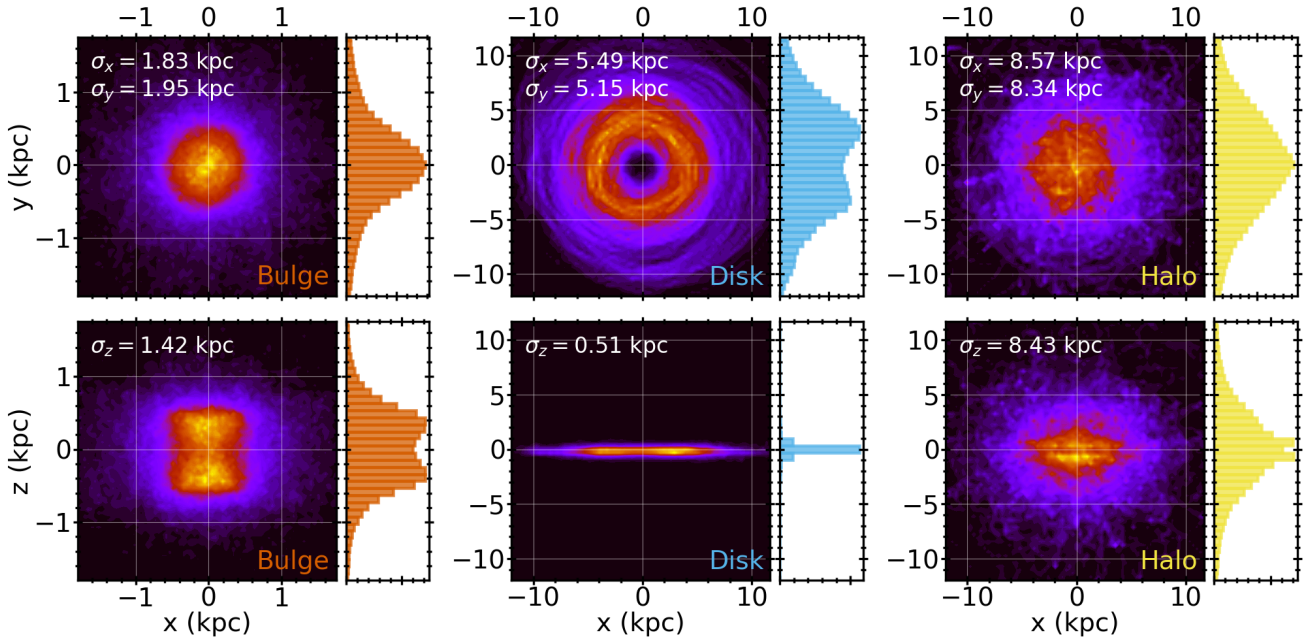


Figure 5: Orbital density projections and marginal profiles of the Milky Way's bulge, disk, and halo after 500 Myr of orbit integration from present day time of the sampled stars from GAIA DR3 data. The first column displays the bulge, the second the disk, and the third the halo. The top row represents the orbital density in the XY plane projection, while the bottom row corresponds to the XZ plane projection. Units are in $\text{star-count} \times \text{yr} \times \text{kpc}^{-2}$. Heatmap scales are not provided as each heatmap is normalized and only relative values are relevant. Each main plot is flanked by its marginal density profile along the respective axis. The σ -values indicate the standard deviation in kiloparsecs for the x , y , and z distributions, offering a statistical measure of the spread in stellar orbits for each component.

(small eccentricity) trajectories and greater pericenter and apocenter distances, consistent with rotational support; and minimal vertical extents, consistent with a thin disk. The halo displays a broad range of eccentric orbits with a very broad distribution of vertical heights, a result consistent with the expected spherical distribution of halo stars.

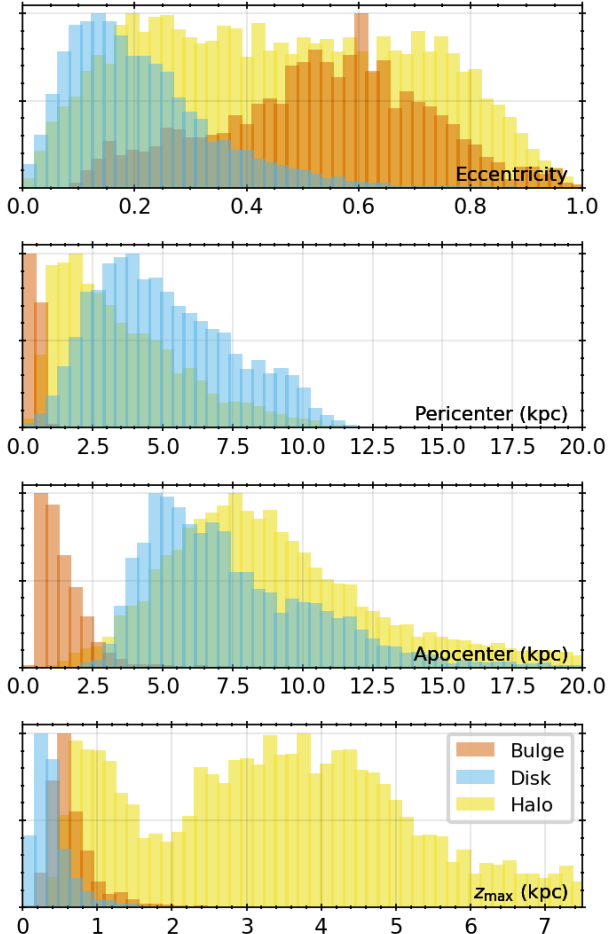


Figure 6: Distribution of orbital parameters for the bulge (red), disk (blue), and halo (yellow) populations of the Milky Way. Top: Eccentricity values, reflecting the shape of the stellar orbits within each galactic component. Middle-Top: Pericenter distances. Middle-Bottom panel: Apocenter distances. Bottom: Average maximum vertical height (z_{\max}) reached above the galactic plane.

Figure 7 shows the distribution of rotational orbital parameters for each galactic component. The top panel shows the distribution of orbital periods. Again, a period cannot be strictly computed for a non-closed orbit. However, an estimate can be provided by extracting periodicity in the signals of the 6D phase-space coordinates and taking its average. From these estimates, we see that the bulge stars tend to have shorter orbital periods, reflecting the more compact mass distribution and the stronger gravitational pull at the galaxy's cen-

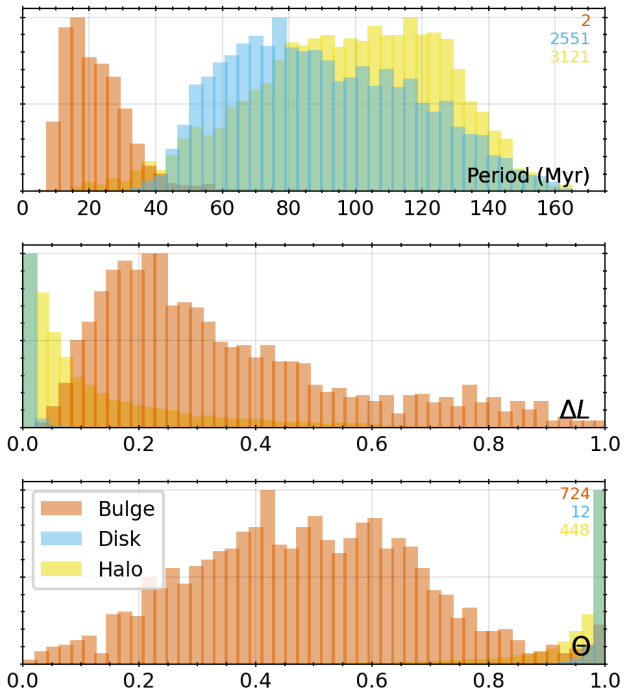


Figure 7: Distribution of rotational orbital parameters for the bulge (red), disk (blue), and halo (yellow) populations of the Milky Way. Top: Orbital period values, with percentage of stars in each component where it could be computed. Middle: ΔL values. Bottom: Θ values. See the main text for the definition of these parameters.

ter. Meanwhile, the disk and halo stars exhibit longer periods, consistent with their wider orbits and the less concentrated mass distribution in these components. For the bulge, the period was computed for all stars but 2. For the disk 2551 stars could not have period computed. For the halo it was 3121. This is due to the orbit integration time being shorter than the orbital period for these stars. Thus, the period distribution for the disk and halo is biased towards shorter periods.

We can further describe the orbital characteristics by computing the angular momentum of each star in each galactic component. We define the angular momentum $\mathbf{L}(t)$ of each star at time t with respect to the galactic center. Let us denote $L(t)$ to be the magnitude of the angular momentum, and $\ell(t)$ its direction, such that $\mathbf{L}(t) = L(t)\ell(t)$. We are interested in the variations of $L(t)$ and $\ell(t)$ throughout the orbit of each star in each galactic component.

To characterize variations in $L(t)$ we define

$$\Delta L = \frac{\sigma_L}{\langle L \rangle}, \quad (3)$$

where $\langle L \rangle$ and σ_L are the mean angular momentum magnitude and standard deviation throughout the or-

bit time. Thus, ΔL represents the relative angular momentum magnitude variation, which serves as a proxy for the complexity of the orbit, as for a two-body-like orbit L is conserved and $\Delta L \approx 0$.

Variations in the angular momentum direction $\ell(t)$ would be indicative of “nutational” motion of the orbital plane, that is, excursions from planar motion. This again would be indicative of complex gravitational interactions beyond a simplified two-body problem. To characterize variations in $\ell(t)$ we define

$$\Theta = \int_{t=0}^T \ell(t) \cdot \langle \ell(t) \rangle_{t=0}^T dt , \quad (4)$$

where $\langle \ell(t) \rangle_{t=0}^T$ is the mean angular momentum direction throughout the orbit. Thus, Θ represents the mean total angular deviation from the mean direction throughout the orbit time. Its values are confined between -1 and 1, with negative values indicating angular momentum inversion. For a two-body-like orbit $\Theta \approx 1$, while for a highly nutating orbit, $\Theta \ll 1$.

Distribution of these magnitudes are represented in the middle and bottom panels of Figure 7. Notably, bulge stars show a broader spread of ΔL and Θ values compared to disk and halo stars. Moreover 774 bulge stars (46.67%) present sign inversion in $\ell(t)$. This suggests that bulge orbits are subject to more complex gravitational influences, possibly due to the bulge’s denser environment. We see that for the disk $\Delta L \approx 0$, $\Theta \approx 1$ and present very few sign inversions (12 stars, 0.14%), indicating that disk stars follow more regular two-body-like orbits. Halo stars present also small ΔL and Θ distribution close to 1, but a greater value of stars with $\ell(t)$ sign inversions: 3121, corresponding to a 40.35% of the halo stars.

4 Discussion and Conclusions

In this study, we used the latest GAIA DR3 dataset to conduct a comprehensive analysis of the stellar orbits across various components of the Milky Way. Using galactocentric coordinates as a fundamental reference frame, we developed an innovative routine for star sampling via GAIA ADQL queries, weighted by a modeled density distribution of our Galaxy. This approach facilitated a preliminary categorization of stars into the galactic bulge, disk, and halo based on their spatial coordinates. Orbits were integrated using the `gala` python package using a smoothed potential approximation for our Galaxy, and each galactic component

was analyzed in terms of its mean orbital parameters.

Regarding our novel routine to sample GAIA stars in galactocentric coordinates, we considered the mass density distribution as a reasonable approximation for the stellar density distribution (used to weight the star selection). Future work may include a direct derivation of the stellar density distribution. Additionally the binning used for star sampling (defining cartesian boxes in galactocentric coordinates and transforming to galactic coordinates) could be further refined to obtain a more homogeneous sample of stars. Also, the classification of stars into galactic components (bulge, disk, halo) was based solely on galactocentric coordinates. A more comprehensive methodology would account for the distinct characteristics of these stellar populations, such as the typically older and more metal-rich nature of bulge stars compared to those in the disk, and similarly for halo stars.

The selection bias toward giant and supergiant stars due to their greater luminosity was noted, which resulted in no main sequence stars and thus a non-representative sample of stellar types.

Our findings indicate that bulge stars exhibit concentrated, eccentric orbits with notable variations in angular momentum. Disk stars’ orbits were observed to be more stable, with minimal vertical displacement from the galactic plane, while halo stars displayed a wide range in eccentricity and significant apocentric distances, indicative of a dynamically excited and widespread component.

5 Data Availability Statement

This work has made use of data from the European Space Agency (ESA) mission *Gaia* (<https://www.cosmos.esa.int/gaia>), processed by the *Gaia* Data Processing and Analysis Consortium (DPAC, <https://www.cosmos.esa.int/web/gaia/dpac/consortium>). Funding for the DPAC has been provided by national institutions, in particular the institutions participating in the *Gaia* Multilateral Agreement.

The results and processed data supporting the findings of this study, along with the code and methodologies employed, are publicly available at the following Github repository: https://github.com/pererossello/MW_toy_model.

References

- J. Bovy. Dynamics and astrophysics of galaxies. <https://galaxiesbook.org/>, 2023. [Online; accessed 11/13/2023].
- Anthony GA Brown, Antonella Vallenari, T Prusti, JHJ De Bruijne, C Babusiaux, M Biermann, OL Creevey, DW Evans, L Eyer, A Hutton, et al. Gaia early data release 3-summary of the contents and survey properties. *Astronomy & Astrophysics*, 649:A1, 2021.
- Jatan Buch, Shing Chau John Leung, and JiJi Fan. Using gaia dr2 to constrain local dark matter density and thin dark disk. *Journal of Cosmology and Astroparticle Physics*, 2019(04):026, 2019.
- OL Creevey, LM Sarro, A Lobel, E Pancino, R Andrae, RL Smart, G Clementini, U Heiter, AJ Korn, M Fouesneau, et al. Gaia data release 3-a golden sample of astrophysical parameters. *Astronomy & Astrophysics*, 674:A39, 2023.
- Lars Hernquist. An analytical model for spherical galaxies and bulges. *Astrophysical Journal, Part 1 (ISSN 0004-637X)*, vol. 356, June 20, 1990, p. 359–364., 356:359–364, 1990.
- Xavier Luri, AGA Brown, LM Sarro, Frédéric Arenou, CAL Bailer-Jones, A Castro-Ginard, J de Bruijne, T Prusti, C Babusiaux, and HE Delgado. Gaia data release 2-using gaia parallaxes. *Astronomy & Astrophysics*, 616:A9, 2018.
- Andrea V Maccio, Greg Stinson, Chris B Brook, James Wadsley, HMP Couchman, Sijing Shen, Brad K Gibson, and Tom Quinn. Halo expansion in cosmological hydro simulations: toward a baryonic solution of the cusp/core problem in massive spirals. *The Astrophysical Journal Letters*, 744(1):L9, 2011.
- Masanori Miyamoto and Ryuzaburo Nagai. Three-dimensional models for the distribution of mass in galaxies. *Astronomical Society of Japan, Publications*, vol. 27, no. 4, 1975, p. 533-543., 27:533–543, 1975.
- Julio F Navarro, Carlos S Frenk, and Simon DM White. A universal density profile from hierarchical clustering. *The Astrophysical Journal*, 490(2):493, 1997.
- Maria Selina Nitschai, Michele Cappellari, and Nadine Neumayer. First gaia dynamical model of the milky way disc with six phase space coordinates: a test for galaxy dynamics. *Monthly Notices of the Royal Astronomical Society*, 494(4):6001–6011, 2020.
- Maria Selina Nitschai, Anna-Christina Eilers, Nadine Neumayer, Michele Cappellari, and Hans-Walter Rix. Dynamical model of the milky way using apogee and gaia data. *The Astrophysical Journal*, 916(2):112, 2021.
- Adrian M. Price-Whelan. Gala: A python package for galactic dynamics. *The Journal of Open Source Software*, 2(18), oct 2017. doi: 10.21105/joss.00388. URL <https://doi.org/10.21105/joss.00388>.
- Timo Prusti, JHJ De Bruijne, Anthony GA Brown, Antonella Vallenari, C Babusiaux, CAL Bailer-Jones, U Bastian, M Biermann, Dafydd Wyn Evans, L Eyer, et al. The gaia mission. *Astronomy & astrophysics*, 595:A1, 2016.
- Thomas P Robitaille, Erik J Tollerud, Perry Greenfield, Michael Droettboom, Erik Bray, Tom Aldcroft, Matt Davis, Adam Ginsburg, Adrian M Price-Whelan, Wolfgang E Kerzendorf, et al. Astropy: A community python package for astronomy. *Astronomy & Astrophysics*, 558:A33, 2013.
- A Vallenari, AGA Brown, T Prusti, JHJ De Bruijne, F Arenou, C Babusiaux, M Biermann, OL Creevey, C Ducourant, DW Evans, et al. Gaia data release 3-summary of the content and survey properties. *Astronomy & Astrophysics*, 674:A1, 2023.

Appendix

The Hernquist bulge is

$$\phi_{\text{bulge}} = -\frac{G m_{\text{bulge}}}{c + \sqrt{x^2 + y^2 + z^2}}, \quad (5)$$

with $m_{\text{bulge}} = 5 \times 10^9 M_{\odot}$ and $c = 1$.

The Nagai-Miyamoto disk is

$$\phi_{\text{disk}} = -\frac{G m_{\text{disk}}}{\sqrt{x^2 + y^2 + (a + \sqrt{b^2 + z^2})^2}}, \quad (6)$$

with $m_{\text{disk}} = 6.8 \times 10^{10} M_{\odot}$, $a = 3$ kpc, and $b = 280$ pc.

The Hernquist bulge is

$$\phi_{\text{nucl}} = -\frac{G m_{\text{nucl}}}{c + \sqrt{x^2 + y^2 + z^2}} \quad (7)$$

with $m_{\text{bulge}} = 2 \times 10^9 M_{\odot}$ and $c = 10$.

The NFW halos is

$$\phi_{\text{halo}} = -\frac{G m_{\text{halo}} \log \left(1 + \frac{\sqrt{\frac{z^2}{c^2} + \frac{y^2}{b^2} + \frac{x^2}{a^2}}}{r_s} \right)}{\sqrt{\frac{z^2}{c^2} + \frac{y^2}{b^2} + \frac{x^2}{a^2}}} \quad (8)$$

with $m_{\text{halo}} = 6 \times 10^{11} M_{\odot}$, and $r_s = 20$ kpc.